Structural transitions and global minima of sodium chloride clusters

Jonathan P. K. Doye*
FOM Institute for Atomic and Molecular Physics, Kruislaan 407, 1098 SJ Amsterdam, The Netherlands

David J. Wales
University Chemical Laboratory, Lensfield Road, Cambridge CB2 1EW, United Kingdom
(Received 28 July 1998)

In recent experiments on sodium chloride clusters, structural transitions between nanocrystals with different cuboidal shapes were detected. Here we determine reaction pathways between the low-energy isomers of one of these clusters, $(NaCl)_{35}Cl^-$. The key process in these structural transitions is a highly cooperative rearrangement in which two parts of the nanocrystal slip past one another on a {110} plane in a $\langle 1\bar{1}0 \rangle$ direction. In this way the nanocrystals can plastically deform, in contrast to the brittle behavior of bulk sodium chloride crystals at the same temperatures; the nanocrystals have mechanical properties which are a unique feature of their finite size. We also report and compare the global potential-energy minima for $(NaCl)_N Cl^-$ using two empirical potentials, and comment on the effect of polarization. [S0163-1829(99)04303-9]

I. INTRODUCTION

There has been much interest in phaselike transitions in clusters. Most of this research has been directed at the finite analogue of the solid-liquid transition,[1] whereas the possibility of transitions between different solid forms has received less attention.[2–4] Some examples are known: when supported metal clusters are observed by electron microscopy, their structure can change between icosahedral, decahedral, and close packed.[5,6] However, the role of the electron beam and the surface is uncertain. Similar transitions have also been suggested for free-atomic clusters of certain sizes, which are driven by entropy differences between the icosahedral, decahedral, and close-packed morphologies.[7–9] However, it is not clear how these changes could be detected even if the large free-energy barriers involved[10] are surmountable.

Coexistence between solidlike isomers of small binary salt clusters was previously described by Rose and Berry.[2] More recently, clear examples of structural transitions have emerged from experiments on NaCl clusters. These clusters have only one energetically favorable morphology: the magic numbers that appear in mass spectra correspond to cuboidal fragments of the bulk crystal (rocksalt) lattice,[11–13] hence the term nanocrystals. Indirect structural information comes from the experiments of Dugourd, Hudgins, and Jarrold, which probed the mobility of size-selected cluster ions. For most $(NaCl)_N Cl^-$ with $N>30$, multiple isomers were detected which were assigned as nanocrystals with different cuboidal shapes.[14] The populations in the different isomers were not initially equilibrated, but slowly evolved, allowing rates and activation energies for the structural transitions between the nanocrystals to be obtained.[15] Based on the small values of the activation energies, Hudgins *et al.* suggested that the rearrangement mechanisms might involve a sequence of surface diffusion steps.

The aim of the present work is to examine this hypothesis by identifying the mechanisms for one of the clusters that was studied experimentally, $(NaCl)_{35}Cl^-$. We also report the global potential-energy minima of $(NaCl)_N Cl^-$ for two different empirical potentials, which enables us to comment on the effects of including polarizabilities and hence induction energies. Methods are outlined in Sec. II, and the global minima are discussed in Sec. III. Then in Sec. IV we describe the mechanism that we found to mediate the structural transitions in $(NaCl)_{35}Cl^-$. Finally, in Sec. V we discuss the implications of this mechanism for the mechanical properties of NaCl nanocrystals and its relevance to other alkali halides.

II. METHODS

A. Searching the potential energy surface

The identification of mechanisms for the structural transitions of $(NaCl)_{35}Cl^-$ presents a considerable challenge to the theoretician, since the half-lives of the least stable isomers are of the order of milliseconds,[15] whereas the time scales that can be probed by conventional molecular-dynamics simulation are only on the order of nanoseconds. The difficulty is that in molecular dynamics or Monte Carlo simulations the system spends most of the time vibrating about a minimum on the potential energy surface (PES), with transitions between minima occurring only rarely. One approach to enhancing the rate of occurrence of rare events, such as these structural transitions, is to bias the system toward transition regions using umbrella sampling[16]; this method is particularly suited to calculating free-energy barriers. Here we use an approach which is ideal for finding reaction pathways for complex processes. Previously it has been used to find a pathway between the face-centered-cubic global minimum and the lowest-energy icosahedral minimum of a 38-atom Lennard-Jones cluster,[17] and to identify relaxation mechanisms in amorphous silicon.[18] Steps are taken directly between minima,[17,19,20] thus allowing large distances on the PES to be traversed. To do this, we first find a transition state connected to the current minimum using the eigenvector-following technique.[21–26] We then calculate the corresponding rearrangement mechanism and thereby obtain the new minimum. Finally, we decide whether to accept the step to the new minimum, typically on the basis of a Metropolis

criterion.[27] By repeating this process the system performs a walk among connected minima on the PES.

The steps between adjacent minima are not biased to go in any particular direction. Nevertheless, by performing an extensive search of the low-lying minima we were able to find paths between the various rocksalt-type isomers of $(NaCl)_{35}Cl^-$. In the process, over 4500 minima and 5500 transition states were characterized. Although there is no guarantee that we have found the shortest or lowest barrier rearrangements between the nanocrystals, we are confident that our paths are good estimates and representative of the optimal paths.

B. Potentials and geometry optimization

Two popular empirical potentials for NaCl were considered in the present work. The first is the Tosi-Fumi parametrization of the Coulomb plus Born-Meyer (C+BM) potential:[28]

$$E=\sum_{i<j}\left(\frac{q_iq_j}{r_{ij}}+A_{ij}e^{-r_{ij}/\rho}\right),$$

where q_i is the charge on ion i, r_{ij} is the distance between ions i and j, and A_{ij} and ρ are parameters.[28] We have also considered the more complex potential fitted by Welch *et al.*,[29] for which the full vector form was given in Ref. 30

$$E=\sum_{i<j}\left(\frac{q_iq_j}{r_{ij}}+A_{ij}e^{-r_{ij}^{\rm eff}/\rho}-\frac{q_i(\boldsymbol{\mu}_j\cdot\mathbf{r}_{ij})}{r_{ij}^3}-\frac{q_j(\boldsymbol{\mu}_i\cdot\mathbf{r}_{ji})}{r_{ij}^3}-3\frac{(\boldsymbol{\mu}_j\cdot\mathbf{r}_{ij})(\boldsymbol{\mu}_i\cdot\mathbf{r}_{ij})}{r_{ij}^5}+\frac{\boldsymbol{\mu}_i\cdot\boldsymbol{\mu}_j}{r_{ij}^3}\right)+\sum_i\frac{\boldsymbol{\mu}_i^2}{2\alpha_i},$$

where

$$r_{ij}^{\rm eff}=\mathbf{r}_{ij}+\frac{\boldsymbol{\mu}_i}{Q_i}-\frac{\boldsymbol{\mu}_j}{Q_j},$$

and $r_{ij}^{\rm eff}=|\mathbf{r}^{\rm eff}|$. [There is a small typographical error in Eq. (3) of Ref. 30.)] The above formulas are given in atomic units. Adopting the notation of Stone,[31] component α of the induced dipole vector at site B due to site A, μ_α^B, is

$$\mu_\alpha^B=\tfrac{1}{2}\sum_{\alpha'}\alpha_{\alpha\alpha'}^BF_{\alpha'}^A(\mathbf{B}),$$

where $\mathbf{A}$ and $\mathbf{B}$ are the position vectors of the respective sites. The total induced moment in the present case is

$$\mu_\alpha^B=\tfrac{1}{2}\sum_{\alpha'}\alpha_{\alpha\alpha'}^B\sum_{A'}\left(\sum_\beta\mu_\beta^{A'}T_{\alpha'\beta}^{A'B}-q^{A'}T_{\alpha'}^{A'B}\right),$$

where

$$T_{\alpha'}^{A'B}=-\frac{R_{\alpha'}}{R^3},$$

$$T_{\alpha'\beta}^{A'B}=\frac{3R_{\alpha'}R_\beta-R^2\delta_{\alpha'\beta}}{R^5},$$

$$\mathbf{R}=\mathbf{B}-\mathbf{A}',\quad\text{and}\quad R=|\mathbf{R}|.$$

Two approaches are available for finding the dipole moments, namely, iterating the equations for μ_α^B to self-consistency or rearranging the equation as

$$\mathbf{M}\boldsymbol{\mu}=\mathbf{Y}\quad\text{so that}\quad\boldsymbol{\mu}=\mathbf{M}^{-1}\mathbf{Y},$$

where $\boldsymbol{\mu}=(\boldsymbol{\mu}^1,\boldsymbol{\mu}^2,\ldots)$. In the present work, matrix inversion was used to obtain the self-consistent dipole moments and the first analytic derivatives of the energy.

The inclusion of polarizabilities in the Welch potential makes this functional form much more expensive to evaluate than the simple C+BM form. Hence we conducted the most extensive searches of the PES with the latter potential, and then reoptimized stationary points and pathways with the Welch form. Global minima were located using a guiding function approach for the Welch potential, as discussed in Sec. III. Transition states were located using a modified eigenvector-following approach. The basic algorithm has been described before,[32,33] and was used in the present work with numerical second derivatives for the Welch potential. We also employed an approach which does not require second derivatives and is more efficient.[34]

III. GLOBAL OPTIMIZATION

Global potential-energy minima were located for $(NaCl)_NCl^-$ up to $N=35$ for both of the empirical potentials described above. We employed the ''basin hopping'' or Monte Carlo minimization[35] technique which has recently been investigated for a variety of atomic and molecular clusters.[8,36–41]

Canonical Monte Carlo (MC) sampling was used to explore the transformed PES, as described elsewhere.[8,36] For the C+BM potential five runs of 5000 MC steps were performed for every cluster size, with each run starting from a random point. Two short runs of 200 steps each were also initiated using the lowest minima for $(NaCl)_{N-1}Cl^-$ and $(NaCl)_{N+1}Cl^-$ as seeds. The maximum step size for the displacement of any Cartesian coordinate was dynamically adjusted to give an acceptance ratio of 0.5 for a temperature corresponding to 316 K (474 K for the larger clusters). Final values for the maximum displacement were typically around 1.5 Å. To restrict the configuration space to bound clusters, we reset the coordinates to those of the current minimum in the Markov chain at each step.[42]

Since the Coulomb potential is long ranged, these clusters actually represent a rather easy global optimization problem because there are fewer minima on their potential-energy surfaces.[7,37,43] Hence we are confident that most of the lowest-energy structures we have identified for the simpler potential are the true global minima. In fact, the lowest minimum was usually the same for each of the five runs at every size considered. The Welch potential is much more time consuming to evaluate, and in this case only three runs of 4000

TABLE I. Energies of the lowest minima found for $(NaCl)_N Cl^-$ clusters with the Coulomb plus Born-Meyer and Welch potentials.

	C+BM		Welch	
N	Energy/eV	PG	Energy/eV	PG
1	−7.712	$D_{\infty h}$	−7.960	$D_{\infty h}$
2	−14.948	$D_{\infty h}$	−15.272	C_{2v}
3	−22.452	C_{3v}	−23.040	C_{3v}
4	−30.204	C_{4v}	−30.871	C_{4v}
5	−37.386	C_{2v}	−38.221	C_1
6	−44.891	C_s	−45.793	C_s
7	−52.511	C_{2v}	−53.456	C_{2v}
8	−60.208	C_{4v}	−61.163	C_{4v}
9	−67.647	C_{3h}	−68.979	C_{3h}
10	−75.141	C_s	−76.398	C_2
11	−82.658	C_s	−84.007	C_1
12	−90.482	C_{4v}	−91.668	C_{4v}
13	−98.672	O_h	−99.756	O_h
14	−105.567	C_s	−106.880	C_s
15	−113.132	C_1	−114.570	C_s
16	−121.086	C_{2v}	−122.497	C_{2v}
17	−128.703	C_{4v}	−129.994	C_{4v}
18	−135.761	C_1	−137.381	C_1
19	−143.611	C_s	−145.255	C_2
20	−151.084	C_s	−152.667	C_s
21	−158.972	C_{4v}	−160.448	C_{4v}
22	−167.158	D_{4h}	−168.576	D_{4h}
23	−174.123	C_s	−175.757	C_1
24	−181.602	C_1	−183.331	D_3
25	−189.525	C_s	−191.227	C_s
26	−197.173	C_{4v}	−198.766	C_{4v}
27	−204.809	C_{2v}	−206.602	C_{2v}
28	−212.385	C_s	−214.152	C_s
29	−219.969	C_s	−221.732	C_1
30	−227.494	C_s	−229.315	C_s
31	−235.584	D_{4h}	−237.305	D_{4h}
32	−242.755	C_s	−244.505	C_s
33	−250.295	C_1	−252.320	C_1
34	−258.304	C_s	−260.187	C_s
35	−265.748	C_s	−267.756	C_s

steps each were performed. We also employed a guiding function technique, as suggested by Hartke,[44] where the simpler C+BM was used for partial geometry optimization followed by relaxation with the full Welch potential in every quench. Once again the same lowest-energy structures were usually found in each of the three runs for every size. The results also agree with calculations performed without a guiding function up to $N=17$, and with those of Phillips *et al.*[30] up to $N=14$, although our energies are systematically lower than those of Ref. 30, presumably due to different unit conversion factors. Our energies and geometries are all well converged with the root-mean-square force reduced to less than 10^{-8} hartree/bohr for every minimum. The most difficult case in this size range appears to be $N=31$, where the $7\times3\times3$ rocksalt global minimum was only found in two out of three runs for the Welch potential.

All the results will be provided in a downloadable format from the Cambridge Cluster Database.[45] The energies of the lowest minima found for both the C+BM and Welch potentials are given in Table I, and the structures are illustrated in Figs. 1 and 2. The lowest ten or so local minima found for the C+BM potential were also relaxed separately under the Welch potential to establish the correspondence between local minima.

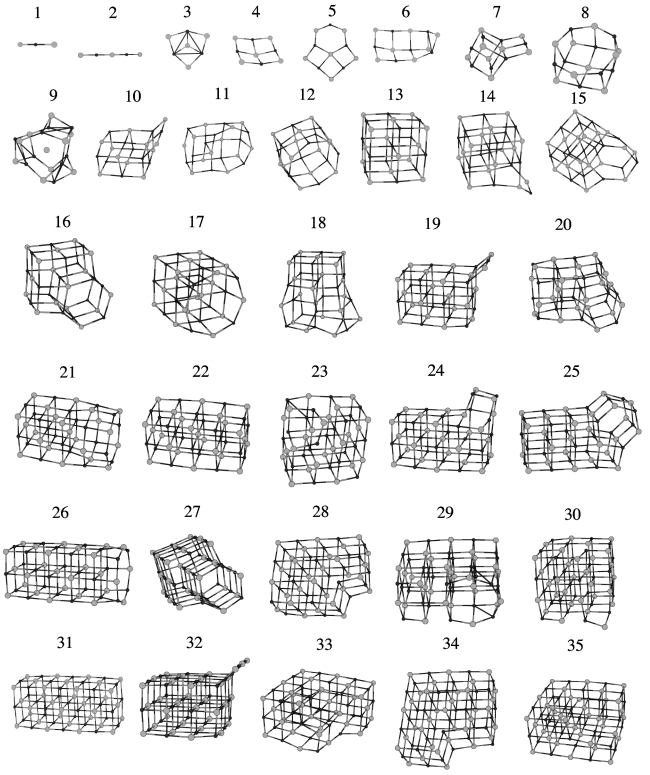

FIG. 1. Global minima for the Coulomb plus Born-Meyer potential. Lines have been drawn using a distance cutoff to guide the eye. The sodium ions are represented by the smaller, darker circles, and the chloride ions by the larger, lighter circles.

For most sizes in the present range the structure of the global potential minimum is the same for the two potentials. However, the global minimum of one potential is only a local minimum for the other potential at $N=6$, 10, 11, 15, 18–20, 23, 24, and 29. For $N=2$ the global minimum is linear for C+BM but somewhat bent for Welch. For $N=5$ the Welch global minimum has lower symmetry than the C+BM structure; the apparent D_{5d} symmetry is actually

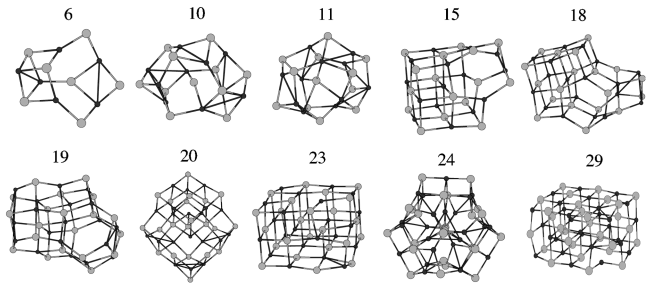

FIG. 2. Global minima for the Welch potential corresponding to local rather than global minima of the Coulomb plus Born-Meyer potential. Lines have been drawn using a distance cutoff to guide the eye. The sodium ions are represented by the smaller, darker circles, and the chloride ions by the larger, lighter circles.

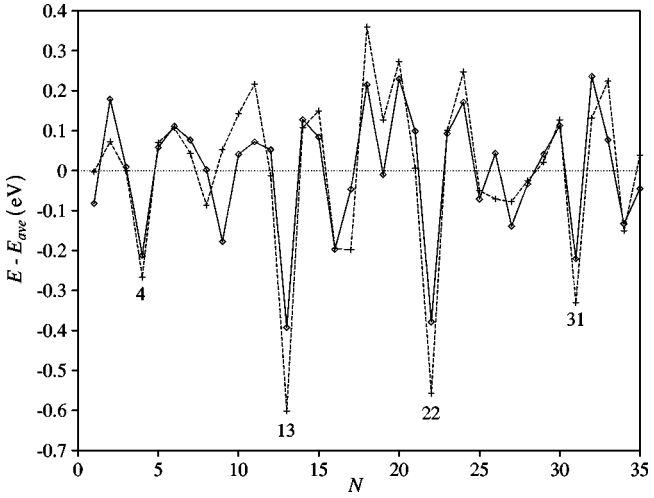

FIG. 3. The energies of the global minima as a function of size for the Welch (solid line) and C+BM (dashed line) potentials. To make the size dependence more clear, we have used a function $E_{\rm ave}=a+bN^{1/3}+cN^{2/3}+dN$ as the energy zero. The coefficients of $E_{\rm ave}$ have been chosen to give the best fit to the energies. For the Welch potential, $a=-0.5014$, $b=0.2139$, $c=0.0926$, and $d=-7.6829$. For the C+BM potential, $a=-1.6782$, $b=1.8878$, $c=-0.2828$, and $d=-7.6360$.

slightly broken on close inspection. The similarity of the results for the two potentials shows that the C+BM form, despite its simplicity, can give a reasonably reliable guide to the structure of these clusters and provides justification for our use of the C+BM potential to perform surveys of the energy landscape.

As expected, the lowest-energy structures have predominantly rocksalt structures, and the particularly stable sizes occur when complete cuboids can be formed (Fig. 3). These sizes ($N=4$, 13, 22, and 31) agree with the magic numbers observed in the mass spectral abundance distributions.[13] It is interesting to note that at a number of sizes when complete cuboids cannot be formed a column of hexagonal rings appears (e.g., $N=16$, 20, 25, and 27). One of the more unusual structures is the $(NaCl)_{24}Cl^-$ global minimum for the Welch potential. It has threefold symmetry, with a trigonal bipyramid in the middle containing three (equatorial) Na^+ ions and two (axial) Cl^- ions.

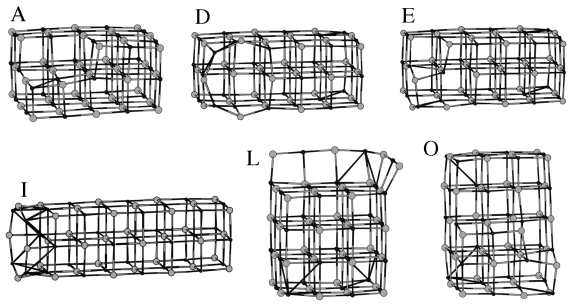

FIG. 4. The lowest energy $(NaCl)_{35}Cl^-$ minima of the four types of nanocrystal for the Coulomb plus Born-Meyer (*A*, *D*, *I*, and *L*) and Welch (*A*, *E*, *I*, and *O*) potentials. *D* and *E* differ only in the position of the vacancy at an Na^+ site. The sodium ions are represented by the smaller, darker circles, and the chloride ions by the larger, lighter circles. The minima are labeled as in Table II.

IV. REARRANGEMENTS OF $(NaCl)_{35}Cl^-$

In the experiments on $(NaCl)_{35}Cl^-$, three peaks were resolved in the arrival time distribution. These peaks were assigned on the basis of calculated mobilities as an incomplete $5\times5\times3$ cuboid, an incomplete $5\times4\times4$ cuboid, and an $8\times3\times3$ cuboid with a single vacancy.[14,15] However, the lowest-energy minima that we found for this cluster could be divided into four types (Table II and Fig. 4), namely, the above three nanocrystals and a $6\times4\times3$ cuboid with a single vacancy. As the latter structure was not considered when the structural assignments were made, its mobility has now been calculated using the exact hard-spheres scattering model.[46,47]

With these data better agreement between the calculated and observed mobilities can be obtained by assigning the

TABLE II. The 15 lowest energy $(NaCl)_{35}Cl^-$ minima for the Coulomb plus Born-Meyer potential. The energies of the minima after reoptimization with the Welch potential are also given.

	Rank		Energy/eV		PG	structure
	C+BM	Welch	C+BM	Welch		
A	1	1	−265.748	−267.756	C_s	$5\times5\times3$
B	2	4	−265.741	−267.653	C_1	$5\times5\times3$
C	3	2	−265.739	−267.721	C_1	$5\times5\times3$
D	4	6	−265.685	−267.582	C_s	$6\times4\times3$
E	5	3	−265.658	−267.656	C_1	$6\times4\times3$
F	6	5	−265.652	−267.588	C_{2v}	$5\times5\times3$
G	7	8	−265.606	−267.524	C_s	$6\times4\times3$
H	8	7	−265.601	−267.573	C_1	$5\times5\times3$
I	9	12	−265.592	−267.476	C_{4v}	$8\times3\times3$
J	10	25	−265.573	−267.417	C_s	$6\times4\times3$
K	11	13	−265.557	−267.467	C_2	$5\times5\times3$
L	12	29	−265.543	−267.400	C_s	$5\times4\times4$
M	13	15	−265.542	−267.465	C_s	$6\times4\times3$
N	14	16	−265.519	−267.445	C_s	$5\times5\times3$
O	15	9	−265.507	−267.502	C_1	$5\times4\times4$

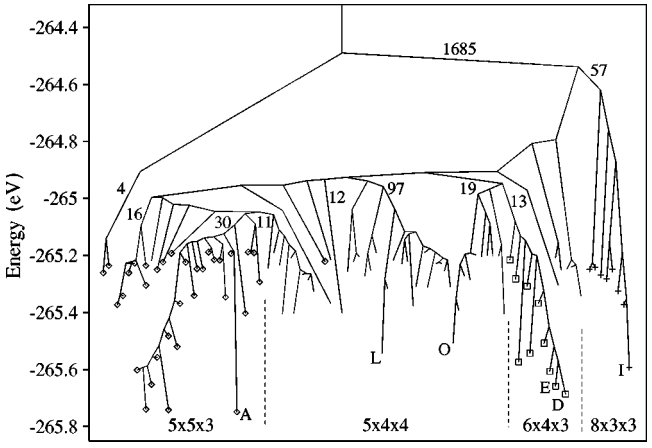

FIG. 5. Disconnectivity graph showing the multiple-funnel character of the $(NaCl)_{35}Cl^-$ PES. The branches that end at the 100 lowest-energy minima are shown. They are marked by the type of structure: $5\times5\times3$, diamonds; $6\times4\times3$, squares; $8\times3\times3$, crosses; and $5\times4\times4$, unlabeled. The dashed lines approximately divide the tree into the different types of nanocrystal. The numbers denote the number of minima in a branch. We also label the six minima that appear in Fig. 4 with the appropriate letter. The energies are for the Coulomb plus Born-Meyer potential.

three experimental peaks to the $6\times4\times3$, $5\times5\times3$ and $8\times3\times3$ nanocrystals in order of increasing drift time.[47] Furthermore, this reassignment gives a better agreement with the energetics. In the experiment the clusters convert to (what we now assign as) the $5\times5\times3$ nanocrystal as time progresses, indicating that this structure has the lowest free energy. In our calculations the global potential-energy minimum is also a $5\times5\times3$ isomer. Moreover, the $6\times4\times3$ nanocrystal is second lowest in energy; it is 0.06 eV (0.10 eV for the Welch potential) above the global minimum, whereas the corresponding value for the lowest energy $5\times4\times4$ isomer is 0.21 eV (0.25 eV).

The disconnectivity graph (or tree)[48,49] in Fig. 5 provides a graphical representation of the PES. It shows which minima are connected by pathways below any given total energy. The end of each line represents a minimum on the PES, and each node occurs at the energy of the transition state which first connects the two (sets of) minima. The tree separates the minima according to the particular rocksalt cuboid quite cleanly. This result shows that the barriers between minima with the same basic cuboidal shape are generally smaller than those between the different types of nanocrystals. This separation holds least well for the $5\times4\times4$ nanocrystals because of the many different ways that the nine vacant sites can be arranged. For example, the two lowest-energy $5\times4\times4$ minima *L* and *O* have very different structures (Fig. 4) and the energy at which the set of minima associated with *O* becomes connected to the $6\times4\times3$ minima is lower than the energy at which it becomes connected to the set of minima associated with *L*. Minimum *O* is also much closer in configuration space to the lowest energy $6\times4\times3$ minimum than it is to minimum *L* (Table III). Another example is provided by the two $5\times5\times3$ isomers on the left of the figure, which are separated by a very large barrier from the rest of the $5\times5\times3$ structures because the ions occupy the opposite lattice sites to the other minima

TABLE III. Details of the pathways between the lowest-energy cuboidal nanocrystals. We give the energy difference between the highest-energy transition state and the lowest-energy minimum of the higher-energy nanocrystal (the barrier), and the path length (Ref. 32) for the paths that minimize these quantities. The values of the barrier in brackets are for the Welch potential, and were obtained by reoptimization of a selection of low-energy pathways; an extensive search of the PES was not conducted with the latter potential. For the $5\times4\times4$ nanocrystal we give the barriers for the minima *L* and *O*, which are the lowest-energy minima of this type for the Coulomb plus Born-Meyer and Welch potentials, respectively.

From	To	Barrier/eV	Path length/Å
$6\times4\times3$	$5\times5\times3$	0.78 (0.69)	33.5
$8\times3\times3$	$5\times5\times3$	1.06 (0.91)	69.8
$(5\times4\times4)L$	$5\times5\times3$	0.62 (0.41)	66.3
$(5\times4\times4)O$	$5\times5\times3$	0.60 (0.54)	46.6
$8\times3\times3$	$6\times4\times3$	1.06 (0.91)	36.3
$(5\times4\times4)L$	$6\times4\times3$	0.63 (0.44)	57.1
$(5\times4\times4)O$	$6\times4\times3$	0.56 (0.54)	14.4
$(5\times4\times4)L$	$8\times3\times3$	1.01 (0.83)	92.6
$(5\times4\times4)O$	$8\times3\times3$	0.97 (0.91)	50.7
$(5\times4\times4)O$	$(5\times4\times4)L$	0.60 (0.43)	42.8

(i.e., the sodium ions, not the chloride ions, are located at the corners of the nanocrystal).

One helpful way to characterize the topography of an energy landscape that has come from the protein folding community is in terms of funnels.[50,51] A funnel is a set of pathways that converge to a low-energy minimum. It has been suggested that a single deep funnel underlies the ability of proteins to fold to a unique native structure. Figure 5 shows that on the $(NaCl)_{35}Cl^-$ PES there are separate funnels corresponding to the $5\times5\times3$, $6\times4\times3$, and $8\times3\times3$ nanocrystals and a number of small funnels associated with the $5\times4\times4$ nanocrystal.

This characterization of the PES helps to explain the initial presence of the metastable isomers in the experiments by Jarrold and co-workers.[14,15] The energy landscape efficiently ''funnels'' high-energy structures into rocksalt-type minima.[52,53] However, the barriers between the different funnels are large, leading to a separation of time scales for relaxation down the PES to a rocksalt structure, and conversion of the metastable nanocrystals to the global minimum. In Ref. 54 we predicted that this behavior would occur for alkali halide clusters.

To understand the mechanisms for the structural transitions, we have visualized many pathways connecting nanocrystals with different dimensions. In virtually all the pathways the major shape changes are achieved by the same type of mechanism. A typical example of this process occurs in the shortest path between the lowest energy $5\times5\times3$ and $6\times4\times3$ isomers. The path involves four sequential transition states [Fig. 6(a)], the first three of which mediate local rearrangements of the empty sites in the $5\times5\times3$ cuboid. The fourth rearrangement causes the major shape change and is depicted in Fig. 7(a). In this ''glide'' mechanism the two halves of the cluster slide past one another on a {110} plane

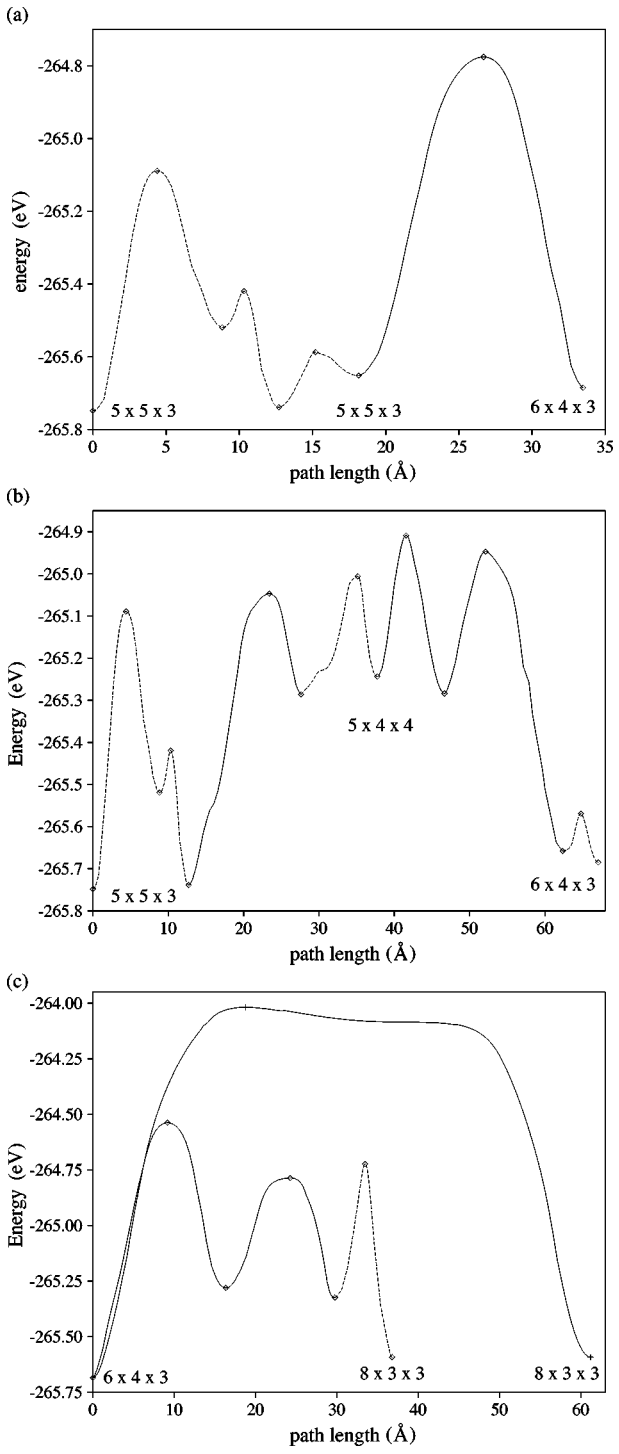

FIG. 6. Energy profiles of pathways between different $(NaCl)_{35}Cl^-$ isomers. (a) The shortest path and (b) the lowest-energy path between the lowest energy $5\times5\times3$ and $6\times4\times3$ isomers. (c) Two pathways between the lowest-energy $6\times4\times3$ and $8\times3\times3$ isomers; the shorter pathway is the pathway with the lowest barrier. The sections of the profiles with solid lines are illustrated in Figs. 7 and 8. The energies are for the Coulomb plus Born-Meyer potential.

in a $\langle 1\bar{1}0 \rangle$ direction. Other examples of this mechanism are illustrated in Figs. 7(b) and 8.

Although the path shown in Figs. 6(a) and 7(a) is the shortest between the lowest-energy $5\times5\times3$ and $6\times4\times3$

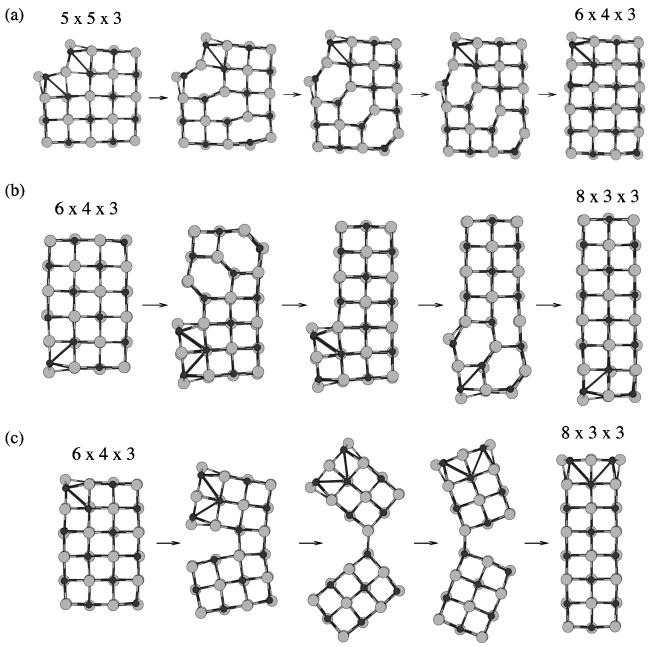

FIG. 7. Portions of the three rearrangement mechanisms corresponding to Figs. 6(a) and 6(c). (a) A glide rearrangement which converts a $5\times5\times3$ isomer into a $6\times4\times3$ isomer. (b) Two glide rearrangements which are part of the lowest-energy path between the $6\times4\times3$ and $8\times3\times3$ isomers. (c) A higher-energy ''hinge'' mechanism which converts a $6\times4\times3$ isomer directly to an $8\times3\times3$ isomer.

minima, it is not the lowest in energy. The latter pathway [Figs. 6(b) and 8] is more complicated; rather than passing directly between the two nanocrystals it goes via a number of $5\times4\times4$ minima, some of which are structurally similar to minimum O. Again the glide mechanism mediates the main structural changes between $5\times5\times3$ and $5\times4\times4$ nanocrystals (top of Fig. 8), and from $5\times4\times4$ to $6\times4\times3$ nanocrystals (bottom of Fig. 8). The former mechanism is not quite so clear cut, since the glide is coupled with local defect motion

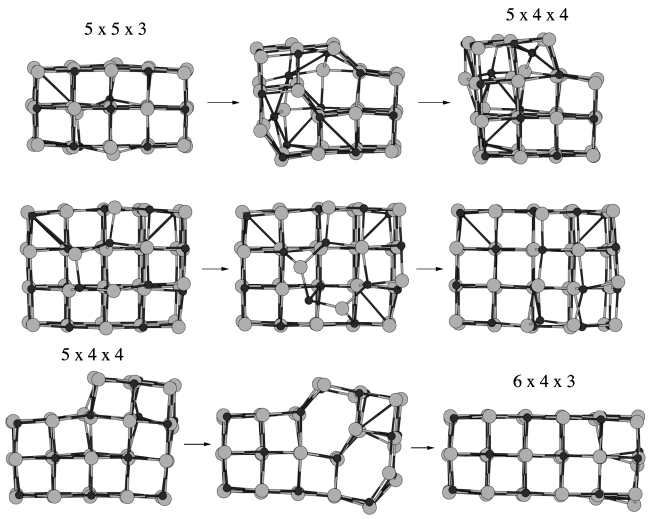

FIG. 8. Three rearrangements from the lowest-energy pathway between the lowest-energy $5\times5\times3$ and $6\times4\times3$ minima, for which the energy profile is shown in Fig. 6(b). The middle frame is the transition state, and on either side are the two minima.

on the far side of the crystal. The middle rearrangement in Fig. 8 actually involves the highest-energy transition state on the pathway. In this rearrangement a triangle of ions slides over the surface of the nanocrystal. The final rearrangement in the pathway (not depicted in Fig. 8) is the conversion of minimum E to minimum D by the motion of a single sodium ion.

The lowest energy pathways to the $8\times3\times3$ nanocrystal all occur via the same transition state. The pathway from the $6\times4\times3$ nanocrystal is illustrated in Figs. 6(c) and 7(b). Two glide rearrangements convert the lowest energy $6\times4\times3$ isomer into an $8\times3\times3$ isomer. In the final rearrangement on this pathway a single sodium ion moves so that the vacancy in the $8\times3\times3$ nanocrystal occupies the site of lowest energy.

It is not hard to see why the glide mechanism is favorable. On either side of the {110} plane are rows of oppositely charged ions [these can be clearly seen on the top face of the nanocrystals in Figs. 7(a) and 7(b)]. When the nanocrystal slides on this plane in the direction of these rows, no ion comes any closer to the nearest ion of the same charge. This situation only holds for {110} planes and the $\langle 1\bar{1}0\rangle$ direction. The activation barrier arises from the loss of some favorable contacts between oppositely charged ions. It is also interesting to note that this plane and direction correspond to the primary slip system for dislocation motion in bulk NaCl crystals.[55]

One other mechanism by which major shape changes can occur is illustrated in Fig. 7(c). In this ''hinge'' process, the two halves of the cluster split apart and rotate about a common edge until they meet up again. Although spectacular this mechanism is unlikely to be relevant to the experiments because the barrier is probably too large [Fig. 6(b)] to be surmountable at the appropriate temperature; the transition state is 1.57 eV (1.21 eV for the Welch potential) above the $8\times3\times3$ minimum.

From the experiments of Jarrold and co-workers, rates and activation energies were obtained for the conversion of the metastable nanocrystals to the global minimum.[15] Therefore, it would be useful if we could make estimates of the activation energies to provide independent support for our results. However, this is nontrivial. There are a number of possible approaches. For a complex process one needs to consider not the energy barrier, but the free-energy barrier. The latter barrier could be computed by umbrella sampling[16] if a suitable order parameter was found which could distinguish the different nanocrystals. The rate of barrier crossing could then be calculated by performing a series of simulations which start from the top of the barrier.[56,57] A second approach is to use a master equation to model the flow of probability between the minima on the PES.[58] However, to achieve reasonable results one probably would need a larger set of minima and transition states than we have obtained here. Furthermore, this approach also requires an expression for the rate constants for transitions between minima. Although these are easily calculated within the harmonic approximation, more accurate rate constants which include the effects of anharmonicity are far harder to obtain. There are also two recently developed techniques which could possibly be applied to calculate the rate constants: the macrostate variational method[59] and the transition path sampling approach of Chandler and co-workers.[60,61]

All these approaches are computationally demanding and beyond the scope of the present work. However, we can obtain an estimate of the activation energy if we make the approximation that the only important path between the nanocrystals is the one with lowest energy. The activation energy can then be equated with the energy difference between the highest-energy transition state on this path and the starting minimum. At absolute zero this energy barrier is equal to the free-energy barrier, however, at nonzero temperatures the free-energy barrier is likely to be reduced by the entropy associated with the multiplicity of paths between the two states. This interplay of energy and entropy has been observed in the free-energy barrier between the lowest-energy face-centered-cubic and icosahedral minima for a 38-atom Lennard-Jones cluster.[10]

In Table III we give our estimates for the activation energies of pathways between the lowest-energy isomers of each cuboidal nanocrystal. In the experiment it was only possible to find the activation energies for rearrangements between the $6\times4\times3$ and $8\times3\times3$ nanocrystals and the $5\times5\times3$ nanocrystal; the values were 0.57 ± 0.05 and 0.53 ± 0.05 eV, respectively.[15] These values are of the same order of magnitude as our estimates of the activation energies (Table III), although somewhat lower than we find for these specific transformations. The differences could be due to the empirical potentials employed or the approximations involved in our estimation of the activation energy, which would probably produce overestimates, as observed. It is also possible that we may not have found the lowest-energy pathways. Furthermore, the barriers are calculated with respect to the lowest-energy minima for a particular type of nanocrystal. However, as the barriers between minima with the same cuboidal shape can be quite large [e.g., in Fig. 6(a) there is a barrier between two $5\times5\times3$ isomers which is 0.66 eV] it is not certain that the nanocrystals in the experiment are in the lowest energy minimum for that shape.

Given these uncertainties, it is not yet possible to use comparison of the experimental and estimated activation energies to provide additional confirmation of the glide mechanism. However, the universality of the glide mechanism among the many low-energy paths that we have discovered strongly suggests that this process does mediate the structural transitions.

Although most of the results in this section are for the C+BM potential those we have obtained using the Welch potential encourage us to believe that the C+BM form provides a reasonable description of the interactions. The global minimum for $(NaCl)_{35}Cl^-$ is the same for the two potentials. Furthermore, the low-energy minima are similar (Table II). There are a few changes in the energetic ordering of the minima; most significantly the $5\times4\times4$ minimum O is significantly lower than minimum L for the Welch potential. It is also interesting to note that the estimates of the activation energy are systematically lower when the Welch potential is used (Table III), bringing the values closer to those found in experiment.[15]

V. DISCUSSION

At the transition state of the glide mechanism there are stacks of hexagonal rings perpendicular to the direction of

sliding (Fig. 7). Hexagonal rings are a common motif in small alkali halide clusters,[30] and when the ratio of the cation to anion size is smaller than for NaCl, e.g. in the lithium halides, NaBr and NaI, the hexagonal structures are more stable than for NaCl.[62] Hence the glide mechanism might be even more favorable in these systems. To prove this supposition, calculations similar to those in this paper could be performed. Furthermore, if this suggestion is correct the dependence of the kinetics of structural transformation on the particular alkali halide could be then used as an experimental test of the mechanism we have found here.

As the glide mechanism is a cooperative mechanism, unlike the surface diffusion mechanism originally suggested,[15] it is expected that the barriers for this type of rearrangement would generally increase with size (although as with any cluster property it is likely that specific size effects would also be superimposed on this trend). The structural transitions would become more difficult with increasing size. Again this could probably be used as an experimental test of the mechanism.

The glide mechanism also has implications for the mechanical properties of these nanocrystals. It allows them to deform spontaneously and plastically to a thermodynamically more stable structure; in other words, the nanocrystals are soft. Similar homogeneous slip mechanisms, where whole planes of atoms slide past one another, have been seen in simulations of strained metal nanowires.[63,64] As the barrier to these cooperative processes increases with the area of the sliding surface, they become less feasible as the size of the system increases. For the metal nanowires the increased barrier leads to a change in the slip mechanism to a more localized process, namely, dislocation motion, with increasing size;[64] the dislocations maintain the ductility of the metal nanowire. In contrast, for NaCl nanocrystals, at temperatures relevant to the experiments considered here [7–67 °C (Ref. 14)], dislocation motion is much more difficult than for metals. Therefore, the increasing barrier appears to lead to a dramatic change in mechanical properties. The nanocrystals become harder as their size increases, until a point is reached where an applied stress is more likely to cause fracture than plastic deformation, and the typical brittle behavior of bulk NaCl crystals is recovered.

The mechanical properties of these NaCl nanocrystals provide another example of the unique finite-size properties of clusters. It might be possible to confirm the increased plasticity we predict using a microscope tip to deform NaCl nanocrystals soft landed on a surface.

Previously, Ball *et al.*[52] compared relaxation to the global minimum of $(KCl)_{32}$ with Ar_{19} in terms of ''monotonic sequences''.[52] On this basis the salt cluster was described as a ''structure seeker'' because rapid removal of kinetic energy usually leads to rocksalt structures; in contrast, it is relatively easy to quench Ar_{19} into a defective double icosahedron. The present results for $(NaCl)_{35}Cl^-$ are relevant to this relation between the energy landscape and relaxation dynamics, regardless of whether the glide mechanism is operative in $(KCl)_{32}$.

Assuming that the model $(KCl)_{32}$ cluster discussed elsewhere has a landscape similar to $(NaCl)_{35}Cl^-$, we would expect different cuboidal rocksalt morphologies to lie at the bottom of separate funnels. Relaxation within each funnel is efficient, but relaxation between funnels will probably occur on a much longer time scale. Hence we can call the salt clusters structure seekers if by structure we mean any of the cuboidal minima. By the same token, then, we should perhaps have bunched the defective double icosahedra together with the global minimum for Ar_{19} in the previous study.[52] In fact Ar_{19} is a ''magic number'' cluster with an essentially single funnel landscape, and so Ar_{19} is also quite an efficient structure seeker. A better contrast would be provided by a cluster bound by a short-range potential, where the landscape would be rougher, or by Ar_{38}, whose double funnel landscape we have investigated elsewhere.[8–10,17,49] The point is that the salt cluster relaxes faster down any one funnel than Ar_{19}, but may not reach the global minimum except over a longer time scale.

ACKNOWLEDGMENTS

We would like to thank Alex Shvartsburg and Martin Jarrold for calculating the mobilities of some of the structures and for helpful discussions. D.J.W. is grateful to the Royal Society for financial support. The work of the FOM Institute is part of the scientific program of FOM, and is supported by the Nederlandse Organisatie voor Wetenschappelijk Onderzoek (NWO).

*Present address: University Chemical Laboratory, Lensfield Road, Cambridge CB2 1EW, United Kingdom.

[1] R. S. Berry, T. L. Beck, H. L. Davis, and J. Jellinek, Adv. Chem. Phys. **70**, 75 (1988).
[2] J. P. Rose and R. S. Berry, J. Chem. Phys. **96**, 517 (1992).
[3] L. S. Bartell, J. Phys. Chem. **99**, 1080 (1995).
[4] A. Proykova and R. S. Berry, Z. Phys. D **40**, 215 (1997).
[5] P. M. Ajayan and L. D. Marks, Phys. Rev. Lett. **60**, 585 (1988).
[6] L. D. Marks, Rep. Prog. Phys. **57**, 603 (1994).
[7] J. P. K. Doye, D. J. Wales, and R. S. Berry, J. Chem. Phys. **103**, 4234 (1995).
[8] J. P. K. Doye and D. J. Wales, Phys. Rev. Lett. **80**, 1357 (1998).
[9] J. P. K. Doye, D. J. Wales, and M. A. Miller, J. Chem. Phys. **109**, 8143 (1998).
[10] J. P. K. Doye, M. A. Miller, and D. J. Wales, cond-mat/9808265 (unpublished).
[11] J. E. Campana, T. M. Barlak, R. J. Colton, J. J. DeCorpo, J. R. Wyatt, and B. I. Dunlap, Phys. Rev. Lett. **47**, 1046 (1981).
[12] R. Pflaum, P. Pfau, K. Sattler, and E. Recknagel, Surf. Sci. **156**, 165 (1985).
[13] Y. J. Twu, C. W. S. Conover, Y. A. Yang, and L. A. Bloomfield, Phys. Rev. B **42**, 5306 (1990).
[14] P. Dugourd, R. R. Hudgins, and M. F. Jarrold, Chem. Phys. Lett. **267**, 186 (1997).
[15] R. R. Hudgins, P. Dugourd, J. M. Tenenbaum, and M. F. Jarrold, Phys. Rev. Lett. **78**, 4213 (1997).
[16] G. M. Torrie and J. P. Valleau, Chem. Phys. Lett. **28**, 578 (1974).
[17] J. P. K. Doye and D. J. Wales, Z. Phys. D **40**, 194 (1997).
[18] G. T. Barkema and N. Mousseau, Phys. Rev. Lett. **81**, 1865 (1998).
[19] G. T. Barkema and N. Mousseau, Phys. Rev. Lett. **77**, 4358 (1996).

[20] N. Mousseau and G. T. Barkema, Phys. Rev. E **57**, 2419 (1998).
[21] C. J. Cerjan and W. H. Miller, J. Chem. Phys. **75**, 2800 (1981).
[22] J. Simons, P. Jorgensen, H. Taylor, and J. Ozment, J. Phys. Chem. **87**, 2745 (1983).
[23] D. O'Neal, H. Taylor, and J. Simons, J. Phys. Chem. **88**, 1510 (1984).
[24] A. Banerjee, N. Adams, J. Simons, and R. Shepard, J. Phys. Chem. **89**, 52 (1985).
[25] J. Baker, J. Comput. Chem. **7**, 385 (1986).
[26] J. Baker, J. Comput. Chem. **8**, 563 (1987).
[27] N. Metropolis, A. W. Rosenbluth, M. N. Rosenbluth, A. H. Teller, and E. Teller, J. Chem. Phys. **21**, 1087 (1953).
[28] M. P. Tosi and F. G. Fumi, J. Phys. Chem. Solids **25**, 45 (1964).
[29] D. O. Welch, O. W. Lazareth, G. J. Dienes, and R. Hatcher, J. Chem. Phys. **64**, 835 (1975).
[30] N. G. Phillips, C. W. S. Conover, and L. A. Bloomfield, J. Chem. Phys. **94**, 4980 (1991).
[31] A. J. Stone, *The Theory of Intermolecular Forces* (Clarendon Press, Oxford, 1996).
[32] D. J. Wales, J. Chem. Phys. **101**, 3750 (1994).
[33] D. J. Wales and T. R. Walsh, J. Chem. Phys. **105**, 6957 (1996).
[34] L. J. Munro and D. J. Wales, Phys. Rev. B (to be published 1 February 1999).
[35] Z. Li and H. A. Scheraga, Proc. Natl. Acad. Sci. USA **84**, 6611 (1987).
[36] D. J. Wales and J. P. K. Doye, J. Phys. Chem. A **101**, 5111 (1997).
[37] J. P. K. Doye and D. J. Wales, J. Chem. Soc., Faraday Trans. **93**, 4233 (1997).
[38] J. P. K. Doye and D. J. Wales, New J. Chem. **22**, 733 (1998).
[39] D. J. Wales and M. P. Hodges, Chem. Phys. Lett. **286**, 65 (1998).
[40] F. Y. Naumkin and D. J. Wales, Mol. Phys. **93**, 633 (1998).
[41] F. Y. Naumkin and D. J. Wales, Chem. Phys. Lett. **290**, 164 (1998).
[42] R. P. White and H. R. Mayne, Chem. Phys. Lett. **289**, 463 (1998).
[43] J. P. K. Doye and D. J. Wales, J. Phys. B **29**, 4859 (1996).
[44] B. Hartke, Chem. Phys. Lett. **258**, 144 (1996).
[45] D. J. Wales, J. P. K. Doye, A. Dullweber, and F. Y. Naumkin, The Cambridge Cluster Database, URL http://brian.ch.cam.ac.uk/CCD.html.
[46] A. A. Shvartsburg and M. F. Jarrold, Chem. Phys. Lett. **86**, 261 (1996).
[47] A. A. Shvartsburg (personal communication).
[48] O. M. Becker and M. Karplus, J. Chem. Phys. **106**, 1495 (1997).
[49] D. J. Wales, M. A. Miller, and T. R. Walsh, Nature (London) **394**, 758 (1998).
[50] P. E. Leopold, M. Montal, and J. N. Onuchic, Proc. Natl. Acad. Sci. USA **89**, 8271 (1992).
[51] J. D. Bryngelson, J. N. Onuchic, N. D. Socci, and P. G. Wolynes, Proteins: Struct., Funct., Genet. **21**, 167 (1995).
[52] K. D. Ball, R. S. Berry, R. E. Kunz, F.-Y. Li, A. Proykova, and D. J. Wales, Science **271**, 963 (1996).
[53] J. P. Rose and R. S. Berry, J. Chem. Phys. **98**, 3262 (1993).
[54] J. P. K. Doye and D. J. Wales, J. Chem. Phys. **105**, 8428 (1996).
[55] M. T. Sprackling, *The Plastic Deformation of Simple Ionic Crystals* (Academic Press, London, 1976).
[56] D. Chandler, *Introduction to Modern Statistical Mechanics* (Oxford University Press, Oxford, 1987).
[57] M. J. Ruiz-Montero, D. Frenkel, and J. J. Brey, Mol. Phys. **90**, 925 (1997).
[58] R. E. Kunz and R. S. Berry, J. Chem. Phys. **103**, 1904 (1995).
[59] A. Ulitsky and D. Shalloway, J. Chem. Phys. **109**, 1670 (1998).
[60] C. Dellago, P. G. Bolhuis, F. S. Csajka, and D. Chandler, J. Chem. Phys. **108**, 1964 (1998).
[61] C. Dellago, P. G. Bolhuis, and D. Chandler, J. Chem. Phys. **108**, 9236 (1998).
[62] A. Aguado, A. Ayuela, J. M. López, and J. A. Alonso, Phys. Rev. B **56**, 15 353 (1997).
[63] G. M. Finbow, R. M. Lynden-Bell, and I. R. McDonald, Mol. Phys. **92**, 705 (1997).
[64] M. R. Sørensen, M. Brandbyge, and K. W. Jacobsen, Phys. Rev. B **57**, 3283 (1998).